Bushra A. Hasan
Ahmad A. Hasan

Department of Physics,
College of Science,
University of Baghdad,
Baghdad, IRAQ

Effect of Antimony Oxide Additive on Characteristics of $(SnO_2)_{1-x}(Sb_2O_3)_x$ Composite Thin Films Synthesized by Pulsed-Laser Deposition

Tin:antimony oxides composites have given great attention due to their unique properties and many application in various fields like optoelectronic devices, gas sensors. The synthesis and characterization of $(SnO_2)_{1-x}(Sb_2O_3)_x$ was conducted in order to comprehend the structure and discuss the optical and dielectric properties of this composites. The x-ray showed that the prepared pure tin oxide thin film was had a polycrystalline structure and that the peaks were identical with the tetragonal phase while the peaks were identical with antimony oxide for x=0.1 to x=0.5. The average crystal size along the preferred level of growth of tin oxide as well as of antimony oxide showed non regular change by increasing of antimony oxide content. Optical measurements showed that the prepared films$(SnO_2)_{1-x}(Sb_2O_3)_x$ had a direct E_g^{opt} energy gap of 3.75 eV, which showed a non- regular increasing to 3.95 eV with the increase of antimony oxide content from x = 0.0 to x = 0.5. Dielectric and electrical impedance properties of $(SnO_2)_{1-x}(Sb_2O_3)_x$ composites were studied over the frequency range from 1kHz to 200kHz. The results showed that the dielectric properties of $(SnO_2)_{1-x}(Sb_2O_3)_x$ composites and showed significant dependence upon frequency. The frequency dependence type of AC conductivity obeys the Jonscher's power law.

Keywords: X-ray diffraction; Dielectric properties; Electrical impedance; AC conductivity
Received: 12 February 2025; **Revised:** 6 April 2025; **Accepted:** 13 April 2025

1. Introduction

Thin films synthesizes from transparent conductive oxides (TCOs) exhibit high transparency in the visible region and low resistivity attracts great attentions due to the wide implementations such as infrared reflectors, solar cells, flat panel displays, touch screens, and electrochromic devices [1-4]. TCO materials such as In-doped tin oxide (ITO), Sb-doped tin oxide (ATO), F-doped tin oxide (FTO), or Al-doped zinc oxide (AZO), and Ga-doped zinc oxide (GZO) have been studied in several researches. Among the different transparent conductive oxides materials, Sb-doped SnO_2 films are attending great interest compared with ITO materials due to their good properties like high stabilities of thermal and chemical properties, very good mechanical durability, redundancy, and inexpensive. Hence, ATO thin films considered as hopeful materials that can be substitute the use of ITO as a result of their individual properties like high transparency (~80%) and low resistivity (~10^3 Ω.m) [5]. There are many techniques that can be adopted to synthesized high-quality ATO films, such as chemical vapor deposition thermal evaporation, sputtering, spray pyrolysis, and sol–gel [5-9]. Among the mentioned techniques pulsed laser deposition received great interest due to advantages such as relatively low cost and a simple manufacturing process. So far, several studies have been interested to creating high-performance TCOs. For example, Burgard et al. referred that spin coating method was adopted to synthesized tin oxide doped with antimony thin films with transmittance was 90% at optimum Sn content [10]. Bisht et al. used spray pyrolysis to created Sb-doped SnO_2 and investigated the optical and the electrical properties [11]. Dua et al. used dip coating to deposit Mn-doped SnO_2 and Sb-doped SnO_2 with high transmittance of 81% [12]. Therefore, it is important to demonstrate a novel fabrication technique for preparing solid state bases Sb-doped SnO_2 thin films.

In this work, the synthesis of SnO_2 mixed with Sb-doped Sb_2O_3 thin films using a pulsed-laser deposition (PLD) technique is firstly reported. Then the structural, and optical properties of these thin films at different mixing ratios were examined. PLD technique is adopted due to many of advantages like simplicity, low cost effectiveness, facile operation, and preparing thin films with of nano-size. Also in this paper, dielectric properties of ATO composites were investigated in the frequency range from 1 to 200 kHz.

2. Experimental Part

The SnO_2:Sb_2O_3 composite thin films were deposited on glass substrates by using PLD. The SnO_2:Sb_2O_3 targets were used for film deposition have been prepared by using solid state reaction technique. Highly pure SnO_2 (99.99%) and Sb_2O_3 (99.99%) powders were used for the target preparation. The content of Sb_2O_3 added to the target were x=0, 0.1, 0.2, 0.3, 0.4, and 0.5. Stoichiometric amounts of SnO_2 and Sb_2O_3 were mixed and put in a quartz ampules, evacuated and sealed and left at oven at temperature of 1000 °C for one hour. The obtained materials were ground to a fine powder by using the ball-milling method and were then pressed into pellet form. Nd:YAG laser was used for the preparation of thin

 © ALL RIGHTS RESERVED

films under vacuum of 10^{-2} mbar thickness of 150 nm. A sufficient gap was kept between the target and the substrate so that the substrate holder did not obstruct the incident laser beam. The laser energy range 500 mJ with a constant shoot of 200 was used. The distance between the target and the substrate was 2 cm while the distance between the target and the laser source was 12 cm .When the laser pulses fall on the material surface, temperature increases to the extent of heat and then increase the heat to the degree of ionization (access to the plasma state). In this case, the atoms move from the surface of the material to the substrate. Thus we get a thin film with high degree of adhesion were obtained. The optical interferometer method was used to determine the film thickness (t), which is based on the interference of light beams reflected from the thin film surface and the substrate bottom, using a He-Ne laser with a wavelength of 632.8 nm. The thickness is calculated using the formula [13]:

$$t = \frac{\lambda}{2}\frac{\Delta x}{x} \quad (1)$$

where Δx and x are the transformation between the interference fringe and the distance between the interference fringe, respectively

The structural characteristics of $(SnO_2)_{1-x}(Sb_2O_3)_x$ composites and thin films were checked using a Phillips x-ray diffraction (XRD) instrument with target Cu k_α wavelength 1.5Å, with the scanning angle has in the range 10-70° with speed 2 cm/min, current 20 mA and voltage 40 kV. The optical characteristics were done using UV–visible–NIR spectrophotometer 180 while the wavelength of the device 190-1100 nm were used to determine both the absorbance and the transmittance of the $(SnO_2)_{1-x}(Sb_2O_3)_x$ thin films which were prepared by PLD.

The optical parameters were estimated using the following relations [14,15]:

$$(\alpha h\nu) = B(h\nu - Eg)^r \quad (2)$$

$$k = \frac{\alpha\lambda}{4\pi} \quad (3)$$

$$n = \sqrt{\frac{4R}{(R-1)^2} - k^2} - \frac{(R+1)}{(R-1)} \quad (4)$$

$$R = \frac{(n-1)^2 + k^2}{(n+1)^2 + k^2} \quad (5)$$

$$\varepsilon_r = n^2 - k^2 \quad (6)$$

$$\varepsilon_i = 2nk \quad (7)$$

The dielectric properties were investigated in the range 1-200 kHz using LCR meter. The dielectric constant (ε_1) is given by [16]:

$$\varepsilon_1 = \frac{C_p}{C_o} \quad (8)$$

where, C_p and C_o are the capacitance of material and in a vacuum, respectively. The dielectric loss (ε_2) is calculated by:

$$\varepsilon_2 = \varepsilon_1 \tan\delta \quad (9)$$

where tan δ is displacement

The A.C. electrical conductivity is determined by:

$$\sigma_{a.c} = \varepsilon_2 \omega \varepsilon_o \quad (10)$$

where ω is the angular frequency

3. Results and Discussion

3.1 Structural analysis

The XRD patterns of $(SnO_2)_{1-x}(Sb_2O_3)_x$ thin films deposited with various composition are shown in Fig. (1). The crystalline structure was analyzed and the (hkl) values were obtained throughout the diffracted x-ray intensity. The structural examination of the main diffraction peaks referred that these peaks are tetragonal rutile-type structure whose unit cell contains six atoms, two tin and four oxygen, displaying an octahedral coordination of the Sn. Millar indices (hkl) of the characteristic of x-ray diffraction put in table (1). From the same figure, all the diffraction peaks present pure tin oxide thin films were identical with tetragonal with the main plane of crystal growth along (110) and (101) located at 2θ of 26.6° and 33.7°. Peaks of secondary phase (monoclinic Sb_2O_5 phase corresponded to antimony oxide) were observed within the detection limits by increasing of antimony content. The creation of the secondary phase affirms the presence of temporal middle phase meanwhile processing of the mixed-oxide. The same figure declared that the intensity of tin oxide began to reduce as antimony oxide content increases also the addition of Sb_2O_3 lead convert the plane of crystal growth.

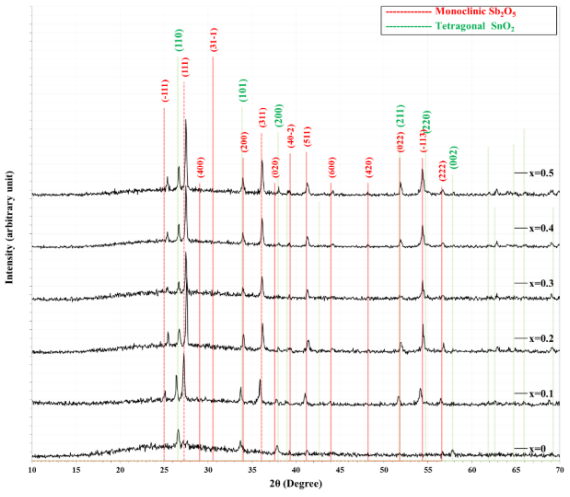

Fig. (1) XRD patterns of $(SnO_2)_{1-x}(Sb_2O_3)_x$ composite thin films

The crystallite size (C.S) of $(SnO_2)_{1-x}(Sb_2O_3)_x$ composites has been measured using the following Debye-Scherrer equation [17]:

$$C.S = \frac{A'\lambda}{\beta\cos\theta} \quad (11)$$

 © ALL RIGHTS RESERVED

Here, A', λ, β, and θ represent constant with value 0.9, the wavelength of the x-ray (1.54Å), full-width at half maximum (FWHM) and Bragg's diffraction angle, respectively

The calculated crystallite size is illustrated table (1). The crystallite size along the plane (110) was 33.9 nm, while the crystallite sizes along the plane (111) were 31.4, 36.6, 43.9, 36.6 and 31.4 nm for x=0.1, 0.2, 0.3, 0.4 and 0.5, respectively. It is clear that the addition of Sb_2O_3 lead to increase the crystal size up x=0.3 but then the crystallite size get to reduce. The reduction of crystallite size occurs due to the stress in the composites which prevents the crystal growth due to the ionic radii variation of Sb^{5+} (0.062 nm) and Sn^{4+} (0.069 nm) [18]. Also, the broadening of the diffraction peaks which indicates that the crystallite size of sample is lowered and the incorporation of Sb in the SnO_2 when x=0.2 lattice lead to shift the main diffraction peak (110) towards the lower diffraction angle value (2θ). It was pointed out previously [19] for Sb_2O_3 loaded SnO_2, the characteristics peaks of the SnO_2 phase shift to lower values of 2θ, indicating an increase of the lattice constant. They also noted that the cation/anion concentration ratio is constant and that the SnO_2 crystal structure is retained with a varying Sb/Sn ratio, indicating that Sb is substitutional incorporated into Sn sites in the SnO_2 lattice. This case it is appropriate to suggest that some of the Sn^{4+} ions in the lattice be replaced by Sb^{5+} ions. This was proved by the increase in the lattice constant with the increase of the Sb/Sn ratio, since the ionic radius of Sn^{4+} is larger than that of Sb^{5+}. However, the extra stress was responsible about the shift towards the higher diffraction angle value (2θ) for residual x values. On the other hand, it was observed from Fig. (1) and table (1) that FWHM was observed to increase as the Sb introduced to the host SnO_2 lattice and for high Sb content, i.e., at x=0.1 and 0.5. This was similar to the finding of [20] for Nb_2O_5 doped SnO_2. This effect was attributed to the cation segregation to the surface of the SnO_2 particle. It is believed that the main element tends to concentrate within the crystallites, while the dopant prefers the outermost areas. Therefore, the dopant-rich region inhibits crystallite growth, leading to an increase in FWHM in the XRD peaks. To get the dislocation density δ and strain ε using the following equations was used as follow [17]:

$$\delta = 1/(C.S)^2 \quad (12)$$

$$\varepsilon = \beta\cos(\theta)/4 \quad (13)$$

The microstrain and dislocation density are summarized in table (1). It is observed that the micro strain and dislocation density parameters are found to be inversely proportional with crystal size value.

3.2 Optical Properties

Optical absorbance spectra of ATO composite thin films for different Sb loading (x = 0.0, 0.10, 0.20, 0.3, 0.4 and 0.5) samples is shown in Fig. (2). It is apparent from this figure that the absorbance increases for the wavelength range 300-350 nm whereas it decreases for the wavelength range 350-1100 nm with the increase in loading concentration. It is clearly observed that all samples have intense absorption curves, the high binding energy of exciton is responsible about the location of absorption edge in the range 300-350 nm also the composites samples showed high transmittance in the visible region [21] as well as absorption in near infrared region which is characteristic of extrinsic semiconductors which give powerful significance of n-type loading, which attributed to surface plasmon absorption.

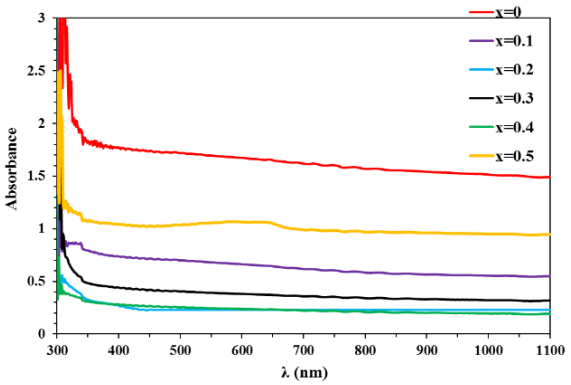

Fig. (2) Absorption spectra of $(SnO_2)_{1-x}(Sb_2O_3)_x$ composites thin films

As proposed by Drude model, which states that the absorption coefficient (α) is directly proportional to the charge carrier density (N) in n-type semiconductors as the following relation [22]:

$$\alpha = \frac{Ne^2}{m_e \tau \omega^2 c n \varepsilon_o} \quad (14)$$

where e and m_e is charge and effective mass of an electron, n is the refractive index of an intrinsic semiconductor, τ is semiconductor relaxation time for free electrons, ε_o vacuum permittivity, c and ω are the speed and frequency of light, respectively

The transmission spectra for $(SnO_2)_{1-x}(Sb_2O_3)_x$ composite thin films for different Sb loading (x = 0.0, 0.1, 0.2, 0.3, 0.4 and 0.5) samples in the wavelength range of 300-1100 nm are shown in Fig. (3), which clearly shows the increase in transmittance due to increase in Sb concentration up x=0.4 and then the transmittance retarded for high loading content. Table (2) shows the values of transmittance of the composite film at 500 nm. It can be concluded that the higher the carrier concentration and hence the higher the conductivity value will be coincided with the lower transmittance. The reduction in transmittance due to high Sb concentration was explained by Ponja et al. [23].

 © ALL RIGHTS RESERVED

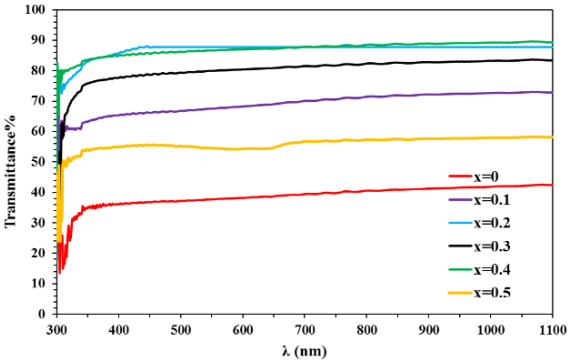

Fig. (3) Transmission spectra of $(SnO_2)_{1-x}(Sb_2O_3)_x$ composite thin films

The transmittance of $(SnO_2)_{1-x}(Sb_2O_3)_x$ composite thin films can be attributed to the excellent electrical properties as a result of high carriers concentration. The relation of Plasmon frequency and its Plasmon wavelength λ_P is directly proportional with the free electron concentration as in the following relation [24]:

$$\omega_p = \frac{4\pi e^2}{m_e \varepsilon_o \varepsilon_\infty} \qquad (15)$$

Here, n denotes the concentration of free electrons, ε_0 and ε_∞ signify the vacuum dielectric constant and high frequency dielectric constants, respectively, m_e symbolizes an electron's effective mass in the conduction band, and e indicates the charge of an electron

It is clearly observed that there is direct relation between of Sb loading and the carrier concentration in ATO composites and inverse relation with Plasmon frequency as shown in Eq. (10).

The optical reflectance spectra of the prepared composite for different loading Sb contents (x= 0.0, 0.1, 0.2, 0.3, 0.4 and 0.5) samples as a function of wavelength ranging from 300 to 1100 nm are shown in Fig. (4). The reflectance in all prepared samples is small for the wavelength range 300-350 nm whereas it shows increase in reflection above the wavelength of 350 nm. The reflectance is found to increase with the increase of loading content up x=0.4 and then the opposite take place.

The variation of the optical absorption coefficient with photon energy (hν) was acquired from the absorbance data in Fig. (2). Many previous research works have used the Tauc formula to calculate the bandgap of SnO_2 samples and referred that SnO_2 is a direct bandgap material [25,26]. The bandgap can be deduced from a plot of $(\alpha h\nu)^2$ as function to photon energy (hν). Perfect linearity of these plots suggests that the samples have direct band transition. The extrapolation of the linear portion of the plot of $(\alpha h\nu)^2$ versus (hν) to zero will give the bandgap value of the samples [27].

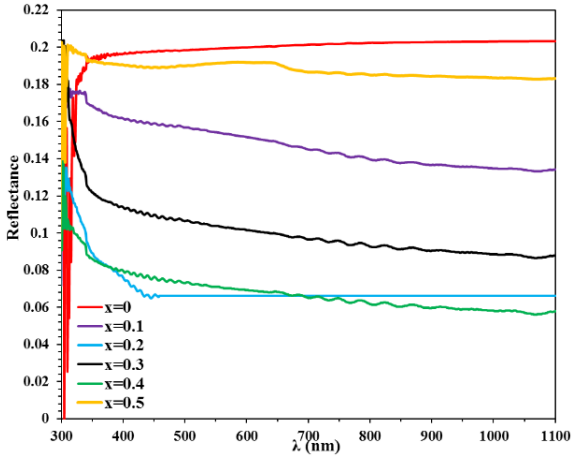

Fig. (4) Reflection spectra of $(SnO_2)_{1-x}(Sb_2O_3)_x$ composite thin films

Figure (5) shows the $(\alpha h\nu)^2$ versus photon energy (hν) plot for pure Sb-doped SnO_2 samples. The linear fits obtained for these plots are also depicted in the figures. The bandgap (E_g) values for $(SnO_2)_{1-x}(Sb_2O_3)_x$ samples with Sb concentrations x = 0.0, 0.1, 0.2, 0.3, 0.4 and 0.5 are 3.1, 3.15, 3.55, 3.45, 3.2 and 2.9 eV, respectively. The analysis of $(SnO_2)_{1-x}(Sb_2O_3)_x$ composite thin films affirm strong depending between bandgap magnitude and the loading level concertation. The energy values were 3.15, 3.55, 3.45 and 3.2 eV corresponding to the loading levels x=0.1, 0.2, 0.3, 0.4, and x=0.5, respectively. All values are rather higher, when compared to calculated value of intrinsic SnO_2 (3.1eV). This agrees with the results of other reports [29]. On the other hand, it is clearly observed that the band gap decreases with the increase of Sb loading for high level loading ratio suggesting that the presence of Sb^{5+}, substituting Sn^{4+} ions in the matrix, encourages a bandgap decrease [28]. The bandgap values are given in table (2).

Another qualification of band gap broadening phenomenon by the rising of Sb loading is given by the Moss-Burstein effect [30]. According to the Pauli's exclusion principle, which states the energy gap will be changed as a results of increasing Sb loading, and a change in Fermi level in the conduction band of an n-type doped semiconductor will be created [31]. High carrier concentration produced occupation of some electrons in the conduction band which giving rise the electrons demand more energy to transport from the valance band to the conduction band, consequently the band gap of $(SnO_2)_{1-x}(Sb_2O_3)_x$ composites will be wide as loading content increases [32].

The extinction coefficient (k) and refractive index (n) versus wavelength in the range 300-1100nm of $(SnO_2)_{1-x}(Sb_2O_3)_x$ composite thin films are plotted in figures (6) and (7). The extinction coefficient and refractive index get to change by increasing of antimony loading level.

 © ALL RIGHTS RESERVED

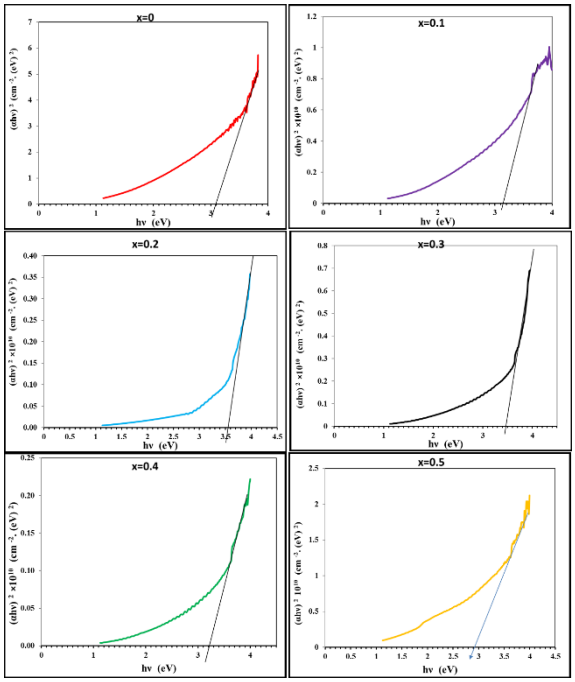

Fig. (5) Variation of $(\alpha h\nu)^2$ with $h\nu$ for $(SnO_2)_{1-x}(Sb_2O_3)_x$ composite thin films prepared in this work

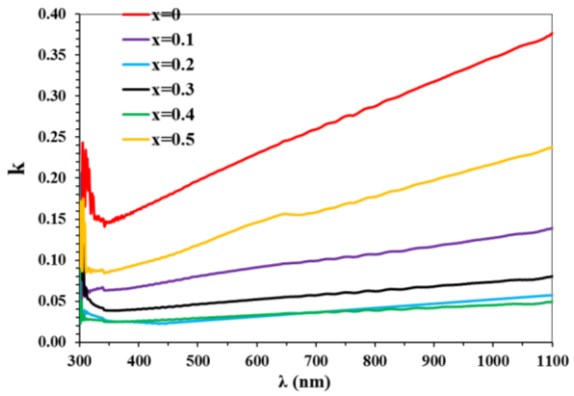

Fig. (6) Variation of extinction coefficient (k) with wavelength for $(SnO_2)_{1-x}(Sb_2O_3)_x$ composite thin films

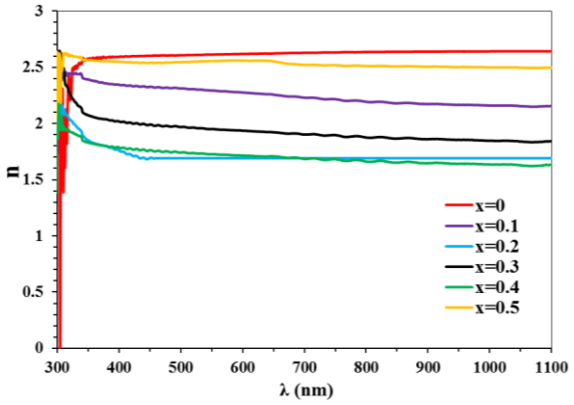

Fig. (7) Variation of refractive index (n) with wavelength of as-deposited $(SnO_2)_{1-x}(Sb_2O_3)_x$ composite thin films

It is observed that the k is increased with increasing wavelength while the refractive index has an opposite behavior in the near infrared region. Figure (6) shows the reduction of extinction coefficient followed by growing at high antimony content indicating the more absorption of light for higher Sb concentration (i.e. x=0.5) due to the generation of free electron or decrement of grain size which increase the grain boundary scattering. The same behavior is also found in the case of refractive index as shown in Fig. (7), which is consistent with the lower transmittance at higher Sb loading level because of the lower value of grain size [33-36].

The complex dielectric constant demonstrates the interaction between electrons and photons. Inductive or capacitive response of an optical material is related to the real parts of the dielectric constant ε_r while resistivity is directly related to the imaginary parts of the dielectric constant ε_i and were determined using extinction coefficient (k) and refractive index (n)

The relations between the real (ε_r) and imaginary (ε_i) parts of the dielectric constant with wavelength in the range 300–1100 nm for ATO composites with different composition (x=0, 0.1, 0.2, 0.3, 0.4 and 0.5), are shown in figures (8) and (9). It is found that ε_r and decreases with the increase of Sb_2O_3 concentration, moreover ε_r and ε_i were found to decrease from 6.826 to 6.472 and from 1.293 to 0.795, respectively, for thin films when Sb_2O_3 concentration increases from 0.0 to 0.5 as shown in table (2).

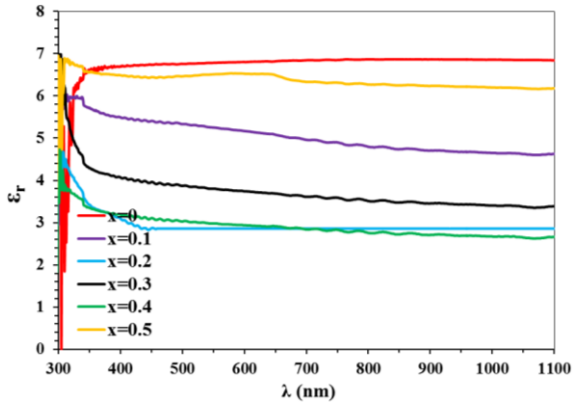

Fig. (8) Variation of ε_r with wavelength for $(SnO_2)_{1-x}(Sb_2O_3)_x$ composite thin films

3.3 Dielectric Measurements

The variation of dielectric constant of the prepared $(SnO_2)_{1-x}(Sb_2O_3)_x$ composite thin films with varying frequency in the range 1 to 200 kHz at constant temperature was investigated. The dielectric constant ε_1 and dielectric loss ε_2 of $(SnO_2)_{0.9}(Sb_2O_3)_{0.1}$, $(SnO_2)_{0.7}(Sb_2O_3)_{0.3}$, and $(SnO_2)_{0.6}(Sb_2O_3)_{0.4}$ composites exhibited strong dependence on frequency (Fig. 10 and 11).

 © ALL RIGHTS RESERVED

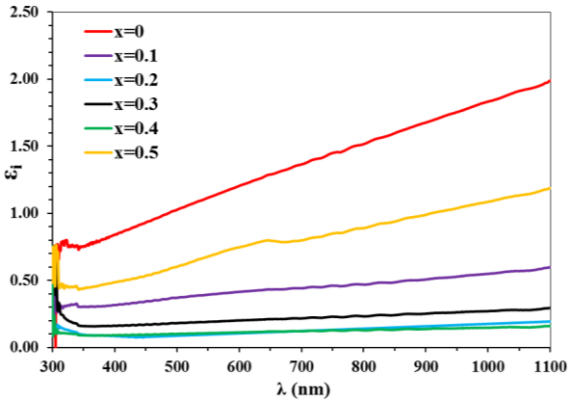

Fig. (9) Variation of ε_i with wavelength for $(SnO_2)_{1-x}(Sb_2O_3)_x$ composite thin films

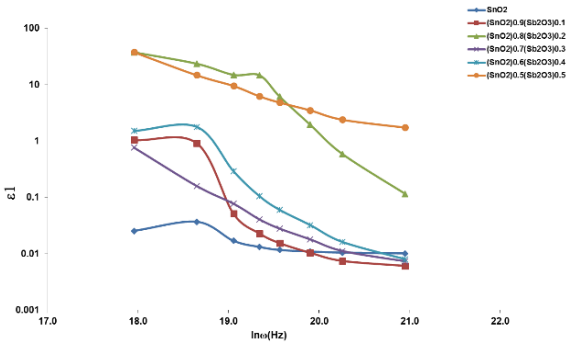

Fig. (10) Frequency-dependent plot of dielectric constant of $(SnO_2)_{1-x}(Sb_2O_3)_x$ composites

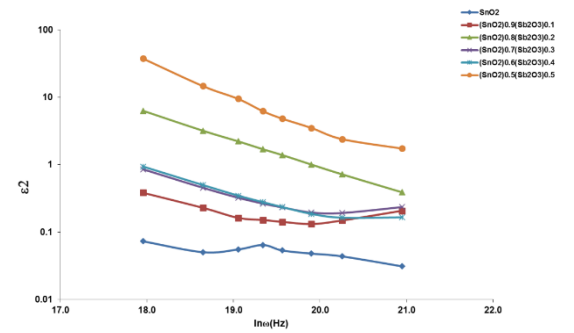

Fig. (11) Frequency-dependent plot of dielectric loss of prepared $(SnO_2)_{1-x}(Sb_2O_3)_x$ composites

The existence of stampede in the low frequency region could be illustrated according to the interfacial polarization. This also suggested the domination of D.C conductivity in the composites sample [37].The values of ε_1 for $(SnO_2)_{0.5}(Sb_2O_3)_{0.5}$ composite was higher than that of residual composites [38,39]. This suggests that the addition of Sb ions, created an oxygen vacancy destroying the vibration of the Sn−O chains, also the difference in the ionic radius or difference between lattice constants which add stress in the lattice [40].

3.4 Cole-Cole Plots

The electrical characteristic of a material is exhibited by the appearance of semicircular arcs in Nyquist plots. Figure (12) shows the complex dielectric constant plots of $(SnO_2)_{1-x}(Sb_2O_3)_x$ composites. It can be seen from Fig. (12) that there exist one semicircular arcs for all composites samples is obtained. This can be explained on the basis of variation of grain size with mixing antimony and tin oxides. The small semicircle obtained in the high frequency region is attributed to the grain conduction while the large semicircle obtained in the low frequency region is due to the grain boundaries. As the particle size decreases the number of grain boundaries increases while the particle size increases the number of grain boundaries reduces.

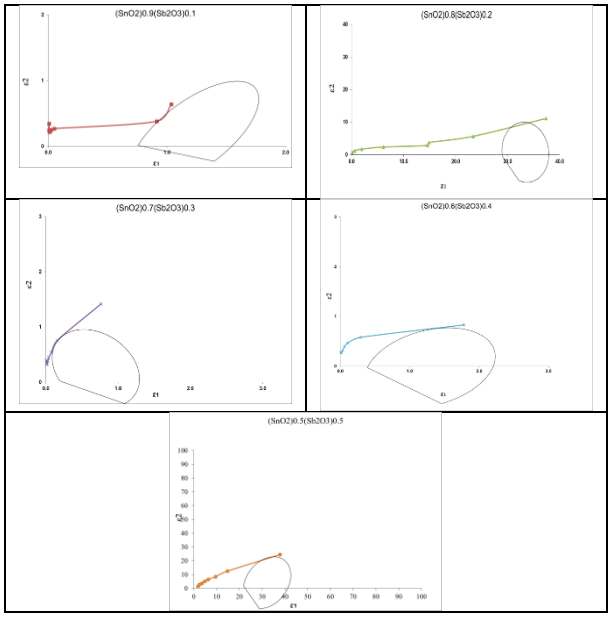

Fig. (12) Cole-Cole plots of $(SnO_2)_{1-x}(Sb_2O_3)_x$ composites

The semicircle belongs to the parallel combination of resistance and capacitance. The plot also suggests that the electrical response consist of one semicircle due to bulk property of the sample [41]. This variation trend of resistance/impedance with antimony content compatible the results obtained from the optical measurements. The values of polarizability α' estimated from the relation [42]

$$\theta = \alpha' \frac{\pi^2}{2} \qquad (16)$$

were 0.157, 0.031, 0.104, 0.052 and 0.029 for x=0.1, 0.2, 0.3, 0.4 and 0.5, respectively. The result declared that polarizability decreases by addition of Sb_2O_3 to the host material which indicate that insertion of high amount Sb (0.3, 0.4, and 0.5) rises the intermolecular forces [43-49]

3.5 A.C Conductivity Measurements

The experimental $\sigma_{A.C}$ values of $(SnO_2)_{1-x}(Sb_2O_3)_x$ composites plots are shown in Fig. (13). The composites samples $(SnO_2)_{0.9}(Sb_2O_3)_{0.1}$,

 © ALL RIGHTS RESERVED

$(SnO_2)_{0.7}(Sb_2O_3)_{0.3}$ and $(SnO_2)_{0.6}(Sb_2O_3)_{0.4}$ prove Jonscher's power law. Figure (13) shows the variation of electrical conductivity $\sigma_{A.C}$ with frequency for various Sb loading levels at room temperature. The ac conductivity increases with frequency for all compositions. Total conductivity of the system is given by

$$\sigma = \sigma_0(T) + \sigma(\omega, T) \quad (17)$$

Here, first term on right hand side represents dc conductivity which is independent of frequency. The second term is pure ac conductivity due to the electron hopping between the metal ions

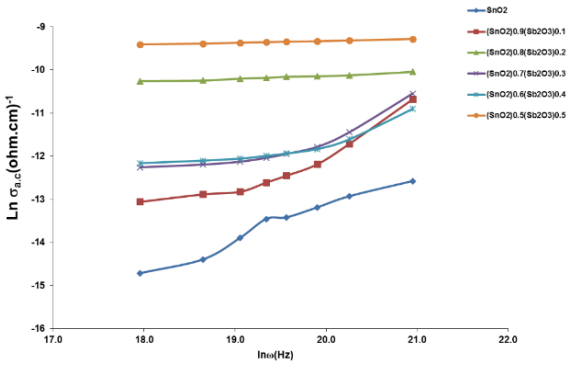

Fig. (13) Frequency dependency plot of σ_{AC} for $(SnO_2)_{1-x}(Sb_2O_3)_x$ composites

It has been observed that ac conductivity increases in gradual way increases with the increase in frequency of applied ac field because the increase in frequency improves the electron hopping frequency. It can also be seen from same figure that conductivity decreases as Sb_2O_3 was added to SnO_2 and then the conductivity increases with the increase on Sb_2O_3. The increase of electrical conductivity of may be attributed to the fact that the dopants of Sb^{5+} are acceptors for SnO_2 and are usually compensated by the formation of oxygen vacancies. Thus, the increase in Sb loading level increases the oxygen vacancies which results in an increase of free electron density and conductivity. However, when Sb^{5+} cannot substitute Sn^{4+}, it will separate to grain boundary interfaces. This separation of Sb^{5+} prevents the building and transportation of electrons and other defects and thereby decreases the conductivity.

The conductivity plot clearly showed two regions the plateau in the low frequency range and conductivity dispersion at high frequency region. This results referred that the σ_{AC} frequency independent in the low range which is known as hopping region which exhibits shifts towards higher-frequency side with the increase antimony oxide [50-52]. The disordering of cations between neighboring sites as well as the space charge are responsible about the increasing of σ_{AC} values with frequency.

4. Conclusions

In concluding remark, $(SnO_2)_{1-x}(Sb_2O_3)_x$ composites have been successfully synthesized. The XRD patterns exhibit the rutile structure for all SnO_2 samples. Monoclinic phase of was detected as secondary phase of Sb_2O_3. The crystallite size have been found to increase by the increasing of Sb_2O_3 up to x=0.3 and then decreases while the micro strain and the dislocation density get to change in opposite to that. The $(SnO_2)_{1-x}(Sb_2O_3)_x$ composite thin films exhibit direct allowed transition and the band gap showed non regular variation with the increase of Sb_2O_3 content. The a.c conductivity shows the frequency and composition dependent behavior. Cole –Cole plot reveals one semicircle for all composites samples.

References

[1] S.H. Park, J.B. Park and P.K. Song, "Characteristics of Al-doped, Ga-dopedand In-doped zinc-oxide films as transparent conducting electrodes inorganic light-emitting diodes", *Curr. Appl. Phys.*, 10 (2010) S488–S490.

[2] D. Slocombe et al., "The Mott transition and optimal performance of transparent conducting oxides in thin-film solar cells", *Energy Enviro. Sci.*, 5 (2012) 5387–5391.

[3] S. Calnan and A.N. Tiwari, "High mobility transparent conducting oxides for thin film solar cells", *Thin Solid Films*, 518 (2010) 1839-1849.

[4] C. Guillen and J. Herrero, "TCO/metal/TCO structures for energy and flexible electronics", *Thin Solid Films*, 520 (2011) 1–17.

[5] T.R. Giraldi et al., "Effect of thickness on the electrical and optical properties of Sb doped SnO_2 (ATO) thin films", *J. Electroceram.*, 13 (2004) 159–165.

[6] K. Ravichandran and P. Philominathan, "Fabrication of antimony doped tin oxide (ATO) films by an inexpensive, simplified spray technique using perfume atomizer", *Mater. Lett.*, 62 (2008) 2980–2983.

[7] J. Kane, H.P. Schweizer and W. Kern, "Chemical vapor deposition of antimony-doped tin oxide films formed from dibutyl tin diacetate", *J. Electrochem. Soc.*, 123 (1976) 270–277.

[8] E.K. Shokr, "Optimization of the electrical and optical properties of Sb–Sn–O thin films", *Semicond. Sci. Technol.,* 15 (2000) 247–253.

[9] S.U. Lee, W.S. Choi and B. Hong, "Synthesis and characterization of SnO_2:Sb film by dc magnetron sputtering method for applications to transparent electrodes", *Physica Scripta*, T129 (2007) 312–315.

[10] D. Burgard, C. Goebbert and R. Nass, "Synthesis of nanocrystalline, redisperable antimony-doped SnO_2 particles for the preparation of conductive,

 © ALL RIGHTS RESERVED

transparent coatings", *J. Sol–Gel Sci. Technol.*, 13 (1998) 789–792.

[11] H. Bisht et al., "Comparison of spray pyrolyzed FTO, ATO and ITO coatings for flat and bent glass substrates", *Thin Solid Films*, 351 (1999) 109–114.

[12] L. Dua and P.K. Biswas, "Synthesis and characterization of nanostructured Mn(II) doped antimony-tin oxide (ATO) films on glass", *Appl. Surf. Sci.*, 280 (2013) 33–41

[13] H. Fizeau, "The Hypotheses Relating to the Luminous Aether, and an Experiment which Appears to Demonstrate that the Motion of Bodies Alters the Velocity with which Light Propagates itself in their Interior", *Philo. Mag.,* 2 (1851) 568–573.

[14] E.A. Davis and N.F. Mott, "Conduction in non-crystalline systems V. Conductivity, optical absorption and photoconductivity in amorphous semiconductors", *Philo. Mag. A*, 22(179) (1970) 903–922.

[15] G.G. MacFarlane and V. Roberts, "Infrared absorption of germanium near the lattice edge", *Phys. Rev.*, 97(6) (1955) 1714–1716.

[16] B.K.P. Scaife, **"Principles of Dielectrics"**, Clarendon Press (Oxford, 1989).

[17] Md.F. Hossain et al., "Transparent conducting SnO_2 thin films synthesized by nebulized spray pyrolysis technique: Impact of Sb doping on the different physical properties", *Mater. Sci. Semicond. Process.*, 121 (2021) 105346.

[18] T. Giraldi et al., "Effect of thickness on the electrical and optical properties of Sb doped SnO_2 (ATO) thin films", *J. Electroceram.*, 131 (2004) 59-65.

[19] M. Kojima, H. Kato and M. Gatto, "Blackening of tin oxide thin films heavily doped with antimony", *Philo. Mag.*, B68 (1993) 215-222.

[20] E.R. Leite, I.T. Weber and E. Longo, "A New Method to Control Particle Size and Particle Size Distribution of SnO_2 Nanoparticles for Gas Sensor Applications", *Adv. Mater.*, 12 (2000) 965-968.

[21] M.L Singla, M.M Shafeeq and M. Kumar, "Optical characterization of ZnO nanoparticles capped with various surfactants", *J. Lumin.*, 129 (2009) 434–438.

[22] Z. Chen et al., "Fabrication of highly transparent and conductive indium-tin oxide thin films with a high figure of merit via solution processing", *Langmuir*, 29(45) (2013) 13836-42.

[23] D. Sapna et al., "Enhanced electrical properties of antimony doped tin oxide thin films deposited via aerosol assisted chemical vapour deposition", *J. Mater. Chem. C*, (2018).

[24] S Vijayalakshmi et al., "Physical properties of zinc doped tin oxide films prepared by spray pyrolysis technique", *J. Phys. D: Appl. Phys.*, 41(3) (2008) 035505.

[25] M. Wang et al., "Sb-doped SnO_2 (ATO) hollow submicron spheres for solar heat insulation coating", *Ceram. Int.*, 47(1) (2020) DOI: 10.1016/j.ceramint.2020.08.162

[26] E.R. Leite et al., "Enhanced electrical property of nanostructured Sb-doped SnO_2 thin film processed by soft chemical method", *Thin Solid Films*, 449 (2004) 67-72.

[27] S. Tsunekawa, T. Fukuda and A. Kasuya, "Blue shift in ultraviolet absorption spectra of monodisperse CeO_{2-x} nanoparticles", *J. Appl. Phys.*, 87 (2000) 1318-1321.

[28] E. Burstein, "Anomalous Optical Absorption Limit in InSb", *Phys. Rev.*, 93 (1954) 632.

[29] E.A. Floriano et al., "Decay of photo-induced conductivity in Sb-doped SnO_2 thin films, using monochromatic light of about bandgap energy", *Appl. Surf. Sci.*, 267 (2013) 164-168.

[30] M. Feneberg et al., "Anisotropic optical properties of highly doped rutile SnO_2: Valence band contributions to the Burstein-Moss shift", *APL Mater.*, 7 (2019) 022508.

[31] M.Z. Ansari N.V. Khare and Kumar, "Synthesis of Cu_2ZnSnS_4 nanoparticles by solvothermal route", *AIP Conf. Proc.*, 1731 (2016) 2–5

[32] M. Sun, J. Liu and B. Dong, "Effects of Sb doping on the structure and properties of SnO_2 films", *Curr. Appl. Phys.*, 20(3) (2020) 462–469.

[33] B.A. Hasan and M.A. Kadhim, "Structure, morphology and optical properties of thermally evaporated Cu_2S thin films annealed at different temperatures", *AIP Conf. Proc.*, 2144 (2019) 030021; https://doi.org/10.1063/1.5123091

[34] A.J. Fadle, M. Ebd Alhur and B.A. Hasan, "Role of ZnO content on the structural, morphology and optical properties of $(NiO)_{1-x}(ZnO)_x$ thin films prepared by pulsed laser deposition technique", 1st Int. Conf. on Pure Sci. (ISCPS-2020), *J. Phys.: Conf. Ser.,* 1660 (2020) 012053 IOP Publishing doi:10.1088/1742-6596/1660/1/012053

[35] B.A. Hasan, D.A. Umran and M.A.K. Mankoshi, "Characterization of CuInSTe/CdS Heterojunctions", *IOP Conf. Series: J. Phys.: Conf. Ser.*, 1032 (2018) 012020.

[36] Y.M. Abbas and A.A. Hasan, "Optical Properties Study of Polypyrrole doped with TiO_2, WO_3, Fe_2O_3 and SnO_2 Nanoparticles", *IOP Conf. Ser.: Mater. Sci. Eng.,* 928 (2020) 072017.

[37] M.R. Biswal et al., "Dielectric and impedance spectroscopic studies of multiferroic BiFe1-xNixO3ceramics", *Adv. Mater. Lett.*, 5(9) (2014) 531–537.

[38] R. Vivekanandan and T.R.N. Kutty, "Hydrothermal synthesis of $Ba(Ti,Sn)O_3$ fine powders and dielectric properties of the

 © ALL RIGHTS RESERVED

corresponding ceramics", *Ceram. Int.*, 14 (1988) 207–206.
[39] G. Arlt, D. Hennings and, G. de With, "Dielectric properties of fine grained barium-titanate ceramics", *J. Appl. Phys.*, 58 (1985) 1619–1625.
[40] M. Willander et al., "Determination of A.C. conductivity of nanocomposite perovskite $Ba_{(1-x-y)}Sr_{(x)}TiFe_{(y)}O_3$ prepared by the sol-gel technique", *J. Crystal. Process Technol.*, 2 (2012) 1–11.
[41] B.N. Parida et al., "A new ferroelectric oxide $Li_2Pb_2Pr_2W_2Ti_2Nb_2O_{30}$: Synthesis and characterization", *J. Phys. Chem. Solids*, 73 (2012) 713–719.
[42] B. Tareev, **"Physics of Dielectric Materials"**, Mir Publisher (Moscow, 1980).
[43] B.A. Hasan et al., "Structural, morphology and optical properties of Al_xSb_{1-x}thin films prepared by Pulsed laser deposition (PLD)", *AIP Conf. Proceed.*, 2372 (2021) 040010.
[44] B.A. Hasan, A.A. Hasan and S.S. Mahmood, "Impact of Zinc Oxide on the Structural and Dielectric Properties of NiO/ZnO Composites", *IJISAE*, 11(5s) (2023) 142–149.
[45] B.A. Hasan and H.H. Issa, "Dielectric properties and A.C electrical conductivity analysis of $(La_2O_3)_{1-x}(ZnO)_x$", *IOP Conf. Ser.: Mater. Sci. Eng.,* 928 (2020) 072003.
[46] Y.M. Abbas and A.A. Hasan, "Dielectric and gas sensing properties of in situ electrochemically polymerized PPy-MgO-WO_3 nanocomposite films", *Iraqi J. Sci.*, 62(9) (2021) 2915-2933.
[47] A.A. Hasan, "Dielectric Study of PVC-LiF Composites Films", *Iraqi J. Sci.*, 62(3) (2021) 861-870.
[48] A.A. Hasan, "Synthesis and Dielectric Properties of MgO:ZnO Composites", *Iraqi J. Sci.*, 63(12) (2022) 5232-5241.
[49] B.A. Hasan, D.A. Uamran and H.H. Issa, "Fabrication, Structure and Dielectric Properties of Fe_2O_3/MgO Composites", *Nonl. Opt. Quantum Opt.*, 58(1-2) (2023) 73-81.
[50] I. Rivera et al., "Divide line between relaxor, diffused ferroelectric, ferroelectric and dielectric", *Solid State Commun.*, 149(3-4) (2009) 172–176.
[51] A.A. Hasan and A.A. Mohammed, "Optical and A.C. Electrical Properties of PMMA/CB, PMMA/G and PMMA/(CB+G) Composites", *Digest J. Nanomater. Biostruct.*, 15(3) (2020) 923-930.
[52] R.H. Khudher and A.A. Hasan, "Effect of Lithium Salts on the Optical Properties of PolyAcrylonitrile/Poly Methyl Methacrylate Blends", *Chem. Methodolog.,* 6 (2022) 872-885.

 © ALL RIGHTS RESERVED

Table (1) XRD data of $(SnO_2)_{1-x}(Sb_2O_3)_x$ thin films composites

ample	2θ (deg.)	FWHM (deg.)	d_{hkl} Exp. (Å)	D (nm)	hkl	Phase	δ ×10^{15} (line/m^2)	ε
0	26.6120	0.2410	3.3469	33.9	(110)	Tet. SnO_2	0.87	0.0044
	33.7000	0.2340	2.6574	35.5	(101)	Tet. SnO_2	0.8	0.003371
	37.8940	0.2520	2.3724	33.3	(200)	Tet. SnO_2	0.9	0.003203
	57.8210	0.2630	1.5934	34.5	(002)	Tet. SnO_2	0.8	0.002078
0.1	25.1583	0.2980	3.5369	27.3	(-111)	Mono. Sb_2O_5	1.3	0.005827
	26.4618	0.2980	3.3656	27.4	(110)	Tet. SnO_2	1.3	0.00553
	27.2812	0.2607	3.2663	31.4	(110)	Mono. Sb_2O_5	1.0	0.004687
	33.7616	0.2979	2.6527	27.9	(101)	Mono. Sb_2O_5	1.3	0.004283
	35.9218	0.3724	2.4980	22.4	(311)	Mono. Sb_2O_5	2.0	0.005013
	37.8212	0.4096	2.3768	20.5	(200)	Tet. SnO_2	2.4	0.005217
	41.0615	0.2979	2.1964	28.5	(511)	Mono. Sb_2O_5	1.2	0.003471
	51.6387	0.4097	1.7686	21.5	(420)	Mono. Sb_2O_5	2.2	0.003695
	54.2086	0.4469	1.6907	20.0	(-113)	Mono. Sb_2O_5	2.5	0.00381
	56.5177	0.3352	1.6270	26.9	(222)	Mono. Sb_2O_5	1.4	0.002721
0.2	25.4562	0.2607	3.4962	31.2	(-111)	Mono. Sb_2O_5	1.0	0.005036
	26.7598	0.3352	3.3288	24.4	(110)	Tet. SnO_2	1.7	0.006149
	27.5791	0.2235	3.2317	36.6	(110)	Mono. Sb_2O_5	0.7	0.003973
	34.0596	0.2607	2.6302	31.9	(101)	Mono. Sb_2O_5	1.0	0.003714
	36.2197	0.2234	2.4781	37.4	(311)	Mono. Sb_2O_5	0.7	0.002981
	37.9702	0.3352	2.3678	25.1	(200)	Tet. SnO_2	1.6	0.004251
	39.3110	0.4842	2.2901	17.4	(40-2)	Mono. Sb_2O_5	3.3	0.005915
	41.4339	0.3352	2.1775	25.3	(511)	Mono. Sb_2O_5	1.6	0.003867
	51.9367	0.4842	1.7592	18.2	(420)	Mono. Sb_2O_5	3.0	0.004338
	54.4320	0.2980	1.6843	30.0	(-113)	Mono. Sb_2O_5	1.1	0.002528
	56.8156	0.2607	1.6191	34.6	(222)	Mono. Sb_2O_5	0.8	0.002103
0.3	25.3818	0.4097	3.5063	19.9	(-111)	Mono. Sb_2O_5	2.5	0.007938
	26.6853	0.4097	3.3379	19.9	(110)	Tet. SnO_2	2.5	0.007537
	27.5047	0.1862	3.2403	43.9	(110)	Mono. Sb_2O_5	0.5	0.00332
	33.9479	0.2980	2.6386	27.9	(101)	Mono. Sb_2O_5	1.3	0.00426
	36.1825	0.2979	2.4806	28.1	(311)	Mono. Sb_2O_5	1.3	0.003979
	39.2737	0.2980	2.2922	28.3	(40-2)	Mono. Sb_2O_5	1.2	0.003644
	41.3222	0.2980	2.1831	28.5	(511)	Mono. Sb_2O_5	1.2	0.003448
	51.8250	0.4469	1.7627	19.8	(420)	Mono. Sb_2O_5	2.6	0.004014
	54.4693	0.2979	1.6832	30.0	(-113)	Mono. Sb_2O_5	1.1	0.002525
0.4	25.4190	0.3352	3.5012	24.3	(-111)	Mono. Sb_2O_5	1.7	0.006485
	26.6853	0.2979	3.3379	27.4	(110)	Tet. SnO_2	1.3	0.00548
	27.5047	0.2235	3.2403	36.6	(110)	Mono. Sb_2O_5	0.7	0.003985
	33.9851	0.3352	2.6358	24.8	(101)	Mono. Sb_2O_5	1.6	0.004786
	36.1825	0.2607	2.4806	32.1	(311)	Mono. Sb_2O_5	1.0	0.003482
	38.0819	0.3725	2.3611	22.6	(200)	Tet. SnO_2	2.0	0.004709
	39.2737	0.4842	2.2922	17.4	(40-2)	Mono. Sb_2O_5	3.3	0.005921
	41.3222	0.4097	2.1831	20.7	(511)	Mono. Sb_2O_5	2.3	0.004741
	51.9367	0.3724	1.7592	23.7	(420)	Mono. Sb_2O_5	1.8	0.003336
	54.4320	0.3724	1.6843	24.0	(-113)	Mono. Sb_2O_5	1.7	0.00316
	56.7039	0.4842	1.6221	18.6	(222)	Mono. Sb_2O_5	2.9	0.003915
0.5	25.4190	0.3724	3.5012	21.9	(-111)	Mono. Sb_2O_5	2.1	0.007205
	26.6853	0.2980	3.3379	27.4	(110)	Tet. SnO_2	1.3	0.005482
	27.5047	0.2607	3.2403	31.4	(110)	Mono. Sb_2O_5	1.0	0.004648
	33.9851	0.3352	2.6358	24.8	(101)	Mono. Sb_2O_5	1.6	0.004786
	36.2197	0.3352	2.4781	24.9	(311)	Mono. Sb_2O_5	1.6	0.004472
	38.1192	0.2235	2.3589	37.6	(200)	Tet. SnO_2	0.7	0.002823
	39.2365	0.4097	2.2943	20.6	(40-2)	Mono. Sb_2O_5	2.4	0.005015
	41.2849	0.4470	2.1850	19.0	(511)	Mono. Sb_2O_5	2.8	0.005177
	51.9367	0.4096	1.7592	21.6	(420)	Mono. Sb_2O_5	2.1	0.003669
	54.3575	0.4841	1.6864	18.4	(-113)	Mono. Sb_2O_5	2.9	0.004114

Table (2) The values of E_g^{opt} and Optical constants at λ=550 nm for $(SnO_2)_{1-x}(Sb_2O_3)_x$ composite thin films

Sample	T%	α (cm^{-1})	k	n	ε_r	ε_i	Eg (eV)
x=0	38.82	47327	0.246	2.624	6.826	1.293	3.10
x=0.1	69.10	18482	0.096	2.254	5.070	0.434	3.15
x=0.2	87.70	6564	0.034	1.691	2.860	0.116	3.55
x=0.3	80.82	10651	0.055	1.920	3.685	0.213	3.45
x=0.4	87.30	6794	0.035	1.706	2.908	0.121	3.2
x=0.5	54.95	29939	0.156	2.549	6.472	0.795	2.9

 © ALL RIGHTS RESERVED